JOURNAL OF SOLID STATE CHEMISTRY 35, 207–214 (1980)

Silver Ionic and Electronic Conductivity in Ag_9GaS_6, Ag_9AlS_6, $AgGaS_2$, $AgAlS_2$, and $AgAl_5S_8$

E. E. HELLSTROM* AND R. A. HUGGINS

Department of Materials Science and Engineering, Stanford University, Stanford, California 94305

Received October 10, 1979; in final form December 3, 1979

Silver ionic and electronic conductivity in phases in the Ag_2S–M_2S_3, M = Al, Ga, systems have been investigated using dc methods with ionically reversible electrodes and ac methods. Measurements on the mixed conductors Ag_9GaS_6 and the new phase Ag_9AlS_6, both with high silver ionic conductivity, the chalcopyrites $AgGaS_2$ and $AgAlS_2$, both with predominate silver ionic conductivity, and the mixed conducting spinel, $AgAl_5S_8$, are reported. In addition, a schematic version of the Ag_2S–Al_2S_3 phase diagram is presented.

Introduction

Ag_2S has been known to be a mixed silver ionic, electronic conductor for many years, and many studies have been made on it (*1*). Phases containing Ag and S, notably Ag_3SX, X = Br, I, also have high ionic conductivities (*1*). The electrical and optical properties of other related ternary phases, notably the chalcopyrite $AgGaS_2$, have been investigated in detail using an electronic semiconductor model (*2*). Recently however, Tell *et al.* (*3*) concluded from galvanic cell emf measurements that $AgGaS_2$ is predominately an ionic conductor.

To assist in the growth of single crystals of $AgGaS_2$, necessary to study its interesting nonlinear optical properties (*2*), the Ag_2S–Ga_2S_3 phase diagram was studied, and the new phase Ag_9GaS_6 was discovered (*4*). It exists in a low-temperature α form and a high-temperature β form (*4*). Almost simultaneously, the analogous phase Ag_9GaSe_6 was reported by Deloume *et al.* (*5*) and Mikkelsen (*6*), the latter of whom suggested that this phase should exhibit silver ionic conductivity. The crystal structures of the high (α) and low (β) temperature forms of Ag_9GaSe_6 have been determined by Deloume *et al.* (*7, 8*).

The existence of the analogous phases Ag_9AlS_6 and Ag_9AlSe_6 has also been communicated (*9*).

The present paper reports on ionic and electronic conductivity in $AgGaS_2$ and Ag_9GaS_6. Phase information along the Ag_2S–Al_2S_3 tie line is also presented, along with results of electrical conductivity measurements on the related phases $AgAlS_2$, Ag_9AlS_6, and $AgAl_5S_8$.

Experimental Methods

A green, optical-quality, single crystal of

* Present address: Department of Solid State Chemistry, Physics Laboratory, State University of Utrecht, P.O. Box 80.000, 3508 TA Utrecht, The Netherlands.

0022-4596/80/140207-08$02.00/0

$AgGaS_2$ was obtained from the Center for Materials Research, Stanford University. Details of the preparation are given in (*10*).

Ag_9GaS_6 was initially prepared by fusing the elements, with a slight S excess, in an evacuated quartz tube whose interior was coated with a pyrolytic graphite layer, and then cooling to room temperature (~100°C/hr). The room-temperature X-ray pattern matched that of the low-temperature α form, with one additional line, later identified as due to sulfur.

It was also prepared by a horizontal zone-leveling reaction of the elements, followed by horizontal zone refining. The material was contained in a graphite boat sealed into an evacuated quartz tube. During the zone leveling, the entire quartz tube was maintained at 415°C with a slight excess of S to control the S partial pressure, and at 465°C during zone refining with an excess of Ag to getter the excess S. In both cases, the moving zone was at 870°C. The room-temperature X-ray pattern of the zone-refined material was that of the α form with no extra lines.

The phases Ag_9AlS_6, $AgAlS_2$, and $AgAl_5S_8$ are sensitive to water vapor, decomposing with the evolution of H_2S on exposure to the atmosphere. Therefore, all preparations, characterizations, and measurements were done within a recirculating, inert atmosphere dry box, or under vacuum using procedures and equipment described elsewhere (*9, 11*).

These three phases were prepared from stoichiometric mixtures of Ag_2S (ICN K&K, New York) and Al_2S_3 (*12*), either by hot pressing (650–800°C) in a graphite die with Al_2O_3 plungers, or by reaction sintering in a sealed quartz tube.

Al_9AlS_6 was black, $AgAlS_2$ was brown when prepared by hot pressing and yellowish brown when prepared by reaction sintering, and polycrystalline $AgAl_5S_8$ was yellowish white.

The Ag_2S–Al_2S_3 phase diagram was investigated using differential thermal analysis (DTA) (Carborundum Model 712) with sealed quartz tubes (0.025 cm^3) whose interiors were coated with pyrolytic graphite as sample containers.

Differential scanning calorimetry (DSC) (Perkin Elmer DSC-2) of the $\alpha \rightleftarrows \beta$ transition in Ag_9GaS_6 was done and employed the melting point of Ga as a temperature reference.

X-ray powder analysis was performed, and the air-sensitive phases were isolated from the atmosphere using Kapton film. KCl or NaCl was used as an internal standard.

Conductivity measurements on the Ag_xAlS_y phases were carried out on disk-shaped, hot-pressed polycrystalline samples fitted for ac measurements with rubbed-on or painted-on (DAG 154) graphite electrodes. The samples of Ag_9GaS_6 were cold pressed. The $AgGaS_2$ crystal was also disk-shaped, and was provided with sputtered Pt electrodes for the ac measurements. Alternate-current measurements

FIG. 1. (a) Two-probe ionic conductivity cell, used in either the constant current or the constant potential mode. (b) Four-probe ionic conductivity cell used for Ag_9GaS_6. Voltage probes II and III measure the potential drop across the sample which is related to the difference in electrochemical potential of silver ions.

were made at 100 mV RMS from 20 to 10^5 Hz using a General Radio 1615 capacitance bridge with a 1632 A tuned null detector.

Direct-current silver ionic conductivity measurements were made using the cells shown schematically in Fig. 1. All phases were measured using the two-probe cell in Fig. 1a, except Ag_9GaS_6, for which the four-probe cell in Fig. 1b was used. The voltage was measured at various values of constant current, at current densities up to 4×10^{-4} A/cm^2 with the potential over the entire cell limited to less than 250 mV.

Results and Discussion

Preparation and Phase Study

Ag_9GaS_6

Material prepared by zone refining with a controlled S partial pressure of ~1 atm contained many internal pores whose walls were covered by S. To remove this excess S, the zone refining was repeated with a Ag bar placed in the quartz tube to act as a S getter. This Ag was not in contact with the Ag_9GaS_6. Even with this getter present, pores still formed in the Ag_9GaS_6, but they were much smaller in size, and their walls were not coated with S. Additionally, Ag whiskers had grown on the upper surface of the recrystallized material due to simultaneous silver ion and electron migration in the silver activity gradient caused by the temperature gradient in the zone-refining system (*13*).

The presence of the pores indicates that S has a higher solubility in molten than in solid Ag_9GaS_6, and is rejected upon freezing. This means that the S activity in molten Ag_9GaS_6 is lower than that set by the Ag + Ag_2S getter equilibrium at 465°C, and therefore, the S getter acts as a S source rather than sink, and cannot control the S activity in molten Ag_9GaS_6. The small amount of S in the pores undoubtedly reacted with the Ag diffusing in the temperature gradient to form Ag_2S, and then the excess Ag precipitated forming whiskers. Ag_2S, as well as Ag and S were, however, not detectable in the X-ray patterns of Ag_9GaS_6.

The $\alpha \rightleftarrows \beta$ phase transition was found to occur at 30 ± 1°C in this study, and at 28 ± 3°C by Skarstad (*14*). It had previously been reported at 35 ± 5°C (*4*).

Ag_2S–Al_2S_3

The phase relations in the previously unreported Ag_2S–Al_2S_3 system are shown schematically in Fig. 2. The system is pseudobinary. The new phase Ag_9AlS_6 was found in this system, and its room-temperature X-ray pattern is analogous to that of α-Ag_9GaS_6 (*4*). It melts congruently at 800 ± 10°C, and on heating, a slight endotherm occurred between room temperature and 50°C, but was not determined more accurately.

The lattice parameters are collected in Table I, along with all structural data known to date on $M_9M'X_6$, M = Ag, Cu; M' = Al, Ga, In; X = S, Se, Te. It is interesting to note that, assuming a phase transition in each of these phases, the transition temperature is higher in the sulfides than in the selenides, just as in the respective binary silver chalcogenides.

The chalcopyrite $AgAlS_2$ reported by Hahn *et al.* (*15*) was found to melt congruently at 1050 ± 10°C and exhibited no high-temperature phase transformation

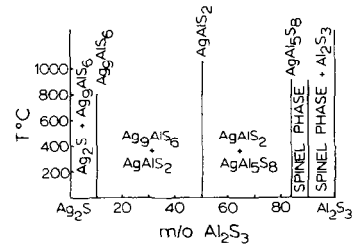

FIG. 2. Phase diagram for Ag_2S–Al_2S_3 (*9*).

prior to melting. The spinel-type phase $AgAl_5S_8$ reported by Flahaut *et al.* (*16*) was found to melt incongruently, with thermal effects at 910 ± 20 and 980 ± 20°C. This spinel phase has a wide range of stoichiometry, extending from below 83.3 to more than 90.0 *m/o* Al_2S_3, as observed in the Li_2S–Al_2S_3 (*11*) and Cu_2S–In_2S_3 (*16*) systems.

Electrical Conductivity

Analysis of dc Ionic Conductivity Measurements

Figure 1a shows a two-probe ionic conductivity cell for measuring the silver ionic conductivity of a phase Ag_xMS_y. Above 149°C where the ionically reversible AgI electrodes have a very high silver ionic conductivity, only a silver ionic current can pass through Ag_xMS_y. The *i–V* characteristics of this cell are due to a combination of: conductivity of the phase Ag_xMS_y; linear $i \cdot R$ polarization losses across the electrodes; and nonlinear, interface ionic-transfer polarization losses due to transfer of Ag ions from phase to phase. This latter polarization often dominates the *i–V* characteristics of the cell, obscuring the ionic conductivity of the phase. To bypass these polarization effects, a four-probe ionic conductivity cell must be used.

A four-probe ionic conductivity cell for measuring silver ionic conduction is shown schematically in Fig. 1b. $RbAg_4I_5$ is a pure silver ionic conductor which can be used over a wide range of temperatures (*17, 18*). While passing a silver ionic current between electrodes I and IV, the potential difference between probes II and III is measured. Since no current flows through the potential probes, no interface ionic-transfer polarization, or $i \cdot R$ potential drop, occurs in these probes, and the ionic conductivity with blocked electronic conductivity can be accurately measured (*19–23*).

The measured potential difference between probes II and III is the difference in electrochemical potential of electrons in the Ag wires, and is related to the differing electrochemical potential of silver ions in Ag_9GaS_6 at the two electrolyte–electrode interfaces. It is given by

$$\phi^{III} - \phi^{II} = \eta_{e'}^{III} - \eta_{e'}^{II} = \eta_{Ag^+}^{3} - \eta_{Ag^+}^{2} \quad (1)$$

where e' are electrons, Ag^+ refers to silver ions, ϕ^k is the electric potential, and η_i^k is

TABLE I

CRYSTALLOGRAPHIC INFORMATION FOR $M_9M'X_6$ PHASES (M = Ag, Cu; M' = Al, Ga, In; X = S, Se, Te)[a]

Phase	Crystal system	Lattice parameters (Å)	Comments	Ref.
Ag_9AlS_6	Orthorhombic	$a_0 = 10.604$, $b_0 = 7.635$ $c_0 = 7.654$	Black, unstable in air	(*9*)
Ag_9AlSe_6	Cubic	$a_0 = 11.114$	Black, unstable in air	(*9*)
Ag_9AlTe_6	—	—	Does not form	
α-Ag_9GaS_6	Orthorhombic	$a_0 = 10.777$, $b_0 = 7.706$ $c_0 = 7.605$	<30°C	(*4*)
β-Ag_9GaS_6	Cubic ($F\bar{4}3m$)	$a_0 = 10.798$	>30°C	(*4*)
β-Ag_9GaSe_6	Cubic ($P2_13$)	$a_0 = 11.126$	<8°C	(*7*)
α-Ag_9GaSe_6	Cubic ($F\bar{4}3m$)	$a_0 = 11.126$	>8°C	(*8*)
Ag_9InS_6	—	—	Does not form	(*9*)
Cu_9GaS_6	—	—	Does not form	(*6*)
Cu_9GaSe_6	—	—	Does not form	(*6*)
Cu_9InS_6	—	—	Does not form	(*32*)

[a] At room temperature, unless otherwise noted.

the electrochemical potential of species i in phase k, where the roman numerals refer to quantities in the Ag leads and the arabic numerals to quantities in Ag_9GaS_6 at the electrode–electrolyte interface.

The electrochemical potential of Ag^+ is given by,

$$\eta_{Ag^+} = \mu_{Ag^+} + q\phi, \qquad (2)$$

where μ_{Ag^+} is the chemical potential of silver ions, and q is the elementary charge. For Ag_9GaS_6, with its high Ag conductivity, $\mu^3_{Ag^+} \cong \mu^2_{Ag^+}$, which together with Eq. (1) and (2) gives

$$\phi^{III} - \phi^{II} = \phi^3 - \phi^2. \qquad (3)$$

The silver ionic conductivity is given by,

$$\sigma_{Ag^+} = \frac{iL}{A(\phi^{III} - \phi^{II})}, \qquad (4)$$

where i is the current, A is the cross-sectional area of the sample, and L is the separation between probes II and III.

Figure 3 shows measured silver ionic and electronic conductivity data for the above phases plotted as log (σT) vs $1/T$. Table II summarizes the activation enthalpies and preexponential factors for conduction. All silver ionic conductivities, except that for $AgAl_5S_8$, were measured using the cells in Fig. 1.

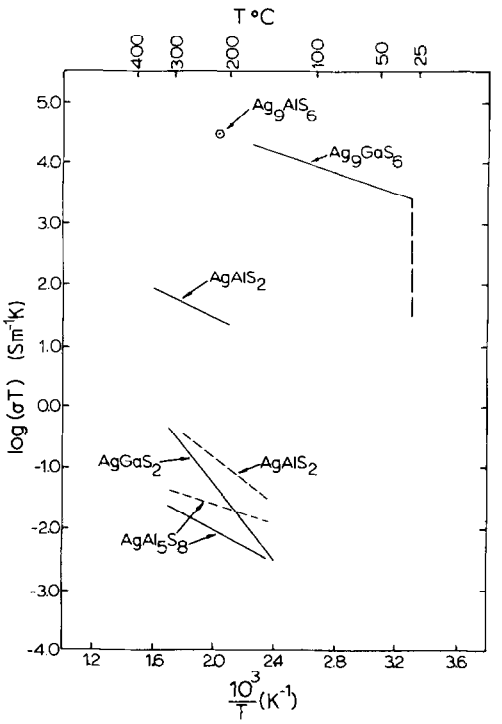

FIG. 3. Silver ionic and electronic conductivity data plotted as log (σT) vs $10^3/T$. Conductivity of $AgAl_5S_8$ measured using ac methods. Dashed lines = electronic conductivity measured with graphite electrodes. Phase transition in Ag_9GaS_6 is shown.

$AgGaS_2$ and $AgAlS_2$

The results reported here were measured on single-crystal $AgGaS_2$ and polycrystalline $AgAlS_2$.

The silver ionic conductivity data shown in Fig. 3 for single-crystal $AgGaS_2$ were measured directly using the cell in Fig. 1a, and were also extracted from ac measurements with ionically blocking Pt electrodes. These data agree within 10%. The almost instantaneous attainment of a steady-state voltage upon changing the current showed that there was negligible interface ionic-transfer polarization when using the cell in Fig. 1a. The silver ionic conductivity was found to be more than 1.5 orders of magnitude greater than the dc-electronic conductivity measured with Pt electrodes. This confirms the conclusion of Tell *et al.* (3) that the silver ionic transport number in $AgGaS_2$ is one, which was based on their emf measurements. The electronic conductivity was not accurately measured.

The silver ionic conductivity in all polycrystalline $AgAlS_2$ samples measured with the two-probe cell had negligible interface ionic-transfer and electrode polarizations. As seen in Fig. 3, the ionic conductivity was greater than the electronic conductivity.

The silver ionic conductivity in the polycrystalline $AgAlS_2$ samples was higher than that of the single-crystal $AgGaS_2$, and had a

TABLE II

ACTIVATION ENTHALPIES AND PREEXPONENTIAL FACTORS FOR SILVER IONIC AND ELECTRONIC CONDUCTIVITY[a]

Sample	σ_{Ag}, σ_{el}	ac, dc	σ_0 ($Sm^{-1}K$)	ΔH (kJ/mole)
Ag_9GaS_6	σ_{Ag}	dc	1.4×10^6	15.8
$AgGaS_2$	σ_{Ag}	dc	1.6×10^5	61.4
$AgGaS_2$	σ_{Ag}	ac	9.0×10^4	59.5
$AgAlS_2$	σ_{Ag}	dc	6.8×10^3	22.6
$AgAlS_2$	σ_{el}	dc	1.1×10^3	37.0
$AgAl_5S_8$	σ_{Ag}	ac	4.0	25.2
$AgAl_5S_8$	σ_{el}	ac	1.0	15.4

[a] All samples were polycrystalline, except Ag_9GaS_6.

lower activation enthalpy for conduction than in $AgGaS_2$.

These differences may be due to slight structural differences in these two chalcopyrite phases, where the c_0/a_0 ratio is 1.80 in $AgAlS_2$ and 1.79 in $AgGaS_2$. However, the large difference in activation enthalpy and the preexponential factor point to two different conduction processes. For the single-crystal $AgGaS_2$, it is clear that the bulk ionic conductivity was measured, while for the polycrystalline $AgAlS_2$ samples, it is thought that conduction occurs along a lower-energy pathway, possibly along grain boundaries.

With the observations of ionic motion in the chalcopyrite structure, it must be recognized that any condition giving rise to a thermodynamic potential gradient in the material may lead to ionic motion to relieve the gradient. This ionic motion may be an explanation for the degradation in optical quality of the chalcopyrites (*24*) when used as nonlinear optical devices with high-energy laser systems. The laser energy gives rise to large stresses (*25*) which may be sufficient to cause shear in the crystal leading to a thermodynamic potential gradient (*26*).

Ionic conductivity must be considered in the Cu chalcopyrites, such as $CuInS_2$ and $CuInSe_2$ (*27*) being investigated for use in solar–voltaic devices. At the elevated temperatures prevalent in solar concentrator systems (*28*), ionic conductivity may lead to diffusional degradation of both homo- and heterojunction devices.

Ag_9GaS_6 and Ag_9AlS_6

The silver ionic conductivity data shown in Fig. 3 were measured on a polycrystalline Ag_9GaS_6 sample using the four-probe cell of Fig. 1b with $RbAg_4I_5$ electrodes. The conductivity was reproducible on heating and cooling. At the $\alpha \rightarrow \beta$ transition, the ionic conductivity of Ag_9GaS_6 increased 100-fold. Ag_9GaS_6 is a mixed conductor; however, the electronic conductivity data which are of the same order of magnitude as the ionic conductivity are not included in Fig. 3 since consistent results have not been obtained.

The silver ionic conductivity of Ag_9AlS_6 was measured using the two-probe cell in Fig. 1a. For the datum reported, interfacial ionic-transfer polarization was negligible as steady state was achieved in less than 15 sec, and the i–V response was reproducible within 5% on reversing and cycling the applied current. The interfacial ionic-transfer polarization became increasingly significant as the temperature was lowered, and below ~200°C, reproducible conductivity values could not be measured.

Since the data for these two phases agree, this implies that the bulk ionic conductivity in both phases was measured, as the high-temperature structures of both phases are expected to be isomorphs, just as the low-temperature phases are, and the identical structures are expected to have nearly the same ionic conductivities.

$AgAl_5S_8$

The electronic conductivity data for $AgAl_5S_8$ shown in Fig. 3 were determined from dc measurements with ionically blocking graphite electrodes. Alternate-current

conductivity measurements were also made with the same electrodes and gave information about both the ionic and electronic conductivity. The ac conductivity data, when plotted in the complex impedance plane, consisted of a high-frequency semicircle passing through the origin, and a low-frequency region which formed a second semicircle over the available frequency range. Both semicircles were centered below the abscissa. The electronic and ionic components of the conductivity were assumed to be in parallel, and the silver ionic conductivity was extracted from the conductivity corresponding to the abscissa intercept between the two semicircles by appropriately subtracting the electronic conductivity. The extracted silver ionic conductivity data are also shown in Fig. 3. In this material, the electronic conductivity was higher than the silver ionic conductivity.

The low conductivity in this spinel corresponds with low ionic conductivity in other spinels, such as that measured directly in $LiFe_5O_8$ using the ionic four-probe technique with 0.6 Li_4SiO_4–0.4 Li_3PO_4 probes (*29*), and inferred from slow solid-state reaction rates for the formation of oxide spinels (*30*). On the other hand, it is not consistent with the contention of Ohachi and Pamplin (*31*) who propose, from the rate at which single crystals of the cubic spinel of composition $Cu_{11}InS_{17}$ grew, that fast ionic motion occurs in this material.

Summary

1. A rudimentary phase diagram for Ag_2S–Al_2S_3 is presented. A new phase Ag_9AlS_6 was found, and the spinel-type phase (nominally $AgAl_5S_8$), was observed to extend from below 83.3 to more than 90.0 *m/o* Al_2S_3.

2. Silver ionic conductivity predominates over the electronic conductivity in the chalcopyrite phases $AgGaS_2$ and $AgAlS_2$. For $AgGaS_2$, $\sigma_{Ag} = 5.3 \times 10^{-5}$ S/m at 200°C.

3. The phases Ag_9AlS_6 and Ag_9GaS_6 are mixed silver ionic, electronic conductors with high silver ionic conductivity. For Ag_9GaS_6, $\sigma_{Ag} = 53$ S/m at 200°C.

4. The spinel phase $AgAl_5S_8$ is a mixed conductor with a low ionic and electronic conductivity. $\sigma_{Ag} = 2.3 \times 10^{-5}$ S/m at 200°C.

Acknowledgments

Helpful discussions with and suggestions from Drs. B. A. Boukamp, B. R. Pamplin, I. D. Raistrick, J. Schoonman, and W. Weppner are gratefully acknowledged. This research was supported in part by the NSF–MRL program through the Center for Materials Research at Stanford University, and by an NSF postdoctoral fellowship (E.E.H.).

References

1. K. FUNKE, *Progr. Solid State Chem.* **11**, 345 (1976).
2. J. L. SHAY AND J. H. WERNICK, "Ternary Chalcopyrite Semiconductors: Growth, Electronic Properties and Applications," Pergamon, Oxford (1975).
3. B. TELL, S. WAGNER, AND H. M. KASPER, JR., *J. Electrochem. Soc.* **124**, 536 (1976).
4. G. BRANDT AND V. KRÄMER, *Mater. Res. Bull.* **11**, 1381 (1976).
5. J. P. DELOUME AND M. ROUBIN, *Compt. Rend. Ser. C* **283**, 747 (1976).
6. J. C. MIKKELSEN, JR., *Mater. Res. Bull.* **12**, 497 (1977).
7. J. P. DELOUME, R. FAURE, H. LOISELEUR, AND M. ROUBIN, *Acta Crystallogr. B* **34**, 3189 (1978).
8. J. P. DELOUME, Crystal structure of α-Ag_9GaSe_6, private communication (1979).
9. E. E. HELLSTROM, Ph.D. dissertation, Stanford University, Stanford, Calif., (1978).
10. R. K. ROUTE, R. S. FEIGELSON, R. J. RAYMAKERS, AND M. M. CHOY, *J. Cryst. Growth* **33**, 239 (1976).
11. E. E. HELLSTROM AND R. A. HUGGINS, *Mater. Res. Bull.* **14**, 881 (1979).
12. E. E. HELLSTROM AND R. A. HUGGINS, *Mater. Res. Bull.* **14**, 127 (1979).

13. H. RICKERT AND C. WAGNER, *Ber. Bunsenges. Phys. Chem.* **67,** 621 (1963).
14. DSC measurements performed on material prepared in this study done by P. M. Skarstad, Medtronic, Inc., Minneapolis, Minn., (1979).
15. H. HAHN, G. FRANK, W. KLINGER, A. D. MEYES, AND G. STÖRGER, *Z. Anorg., Allg. Chem.* **271,** 153 (1953).
16. J. FLAHAUT, L. DOMANGE, M. GUITTARD, M. OURMITCHI, AND J. K. S. KOM, *Bull. Soc. Chim. Fr.* **28,** 2382 (1961).
17. B. B. OWENS AND G. R. ARGUE, *Science* **157,** 308 (1967).
18. J. N. BRADLEY AND P. D. GREENE, *Trans. Faraday Soc.* **63,** 424 (1967).
19. C. WAGNER, "International Committee on Electrochemical Thermodynamics and Kinetics (C.I.T.C.E.), 7th meeting, Lindau," p. 361 (1955).
20. C. WAGNER, *Progr. Solid State Chem.* **10,** 3 (1976).
21. H. RICKERT, *Z. Phys. Chem. N.F.* **23,** 355 (1960).
22. G. J. DUDLEY AND B. C. H. STEELE, *J. Solid State Chem.* **21,** 1 (1977).
23. I. BARTKOWICZ AND S. MROWEC, *Phys. Status Solidi B* **49,** 101 (1972).
24. D. C. HANNA, B. LUTHER-DAVIES, H. N. RUTT, R. C. SMITH, AND C. R. STANLEY, *IEEE J. Quantum Electron.* **QE8,** 317 (1972).
25. B. P. FAIRAND AND A. H. CLAUER, *J. Appl. Phys.* **50,** 1497 (1979).
26. J. P. HIRTH AND J. LOTHE, "Theory of Dislocations," McGraw–Hill, New York (1968), chaps. 12 and 14.
27. J. L. SHAY, S. WAGNER, AND H. M. KASPER, *Appl. Phys. Lett.* **27,** 89 (1975).
28. L. W. JAMES AND R. L. MOON, *Appl. Phys. Lett.* **26,** 467 (1975).
29. G. J. DUDLEY AND B. C. H. STEELE, *J. Electrochem. Soc.* **125,** 1994 (1978).
30. F. S. PETTIT, E. H. RANDKLEV, AND E. J. FELTEN, *J. Amer. Ceram. Soc.* **49,** 199 (1966).
31. T. OHACHI AND B. R. PAMPLIN, *J. Cryst. Growth* **42,** 598 (1977).
32. J. J. M. BINSMA, L. J. GILING, AND J. BLOEM, submitted for publication.